Turkish Journal of Chemistry

http://journals.tubitak.gov.tr/chem/

Research Article

Turk J Chem
(2017) 41: 221 – 232

doi:10.3906/kim-1604-44

Hydrolysis of ammonia borane and hydrazine borane by poly(*N*-vinyl-2-pyrrolidone)-stabilized CoPd nanoparticles for chemical hydrogen storage

Murat RAKAP[1,*], Bayram ABAY[2], Nihat TUNÇ[2]
[1]Maritime Faculty, Yüzüncü Yıl University, Van, Turkey
[2]Department of Chemistry, Yüzüncü Yıl University, Van, Turkey

Received: 15.04.2016 • **Accepted/Published Online:** 10.09.2016 • **Final Version:** 19.04.2017

Abstract: For the first time the synthesis of poly(*N*-vinyl-2-pyrrolidone)-stabilized cobalt-palladium nanoparticles by an easy method, their characterization, and their use as active catalysts for hydrogen release from hydrolysis of ammonia borane and hydrazine borane is reported here. The catalyst is prepared by simultaneous reduction of suitable cobalt and palladium ions by sodium borohydride in the presence of poly(*N*-vinyl-2-pyrrolidone) as a stabilizer. They are characterized by UV-Vis spectroscopy, TEM analysis, X-ray diffraction, and X-ray photoelectron spectroscopy. They provide average turnover frequencies of 30 min^{-1} and 45 min^{-1} in the hydrolysis of ammonia borane and hydrazine borane. They also provide activation energies of 48.6 ± 2 and 50.6 ± 2 kJ mol^{-1} in the hydrolysis of ammonia borane and hydrazine borane.

Key words: Cobalt, palladium, ammonia borane, hydrazine borane, hydrolysis

1. Introduction

In order to overcome energy-related environmental global problems, hydrogen is seen one of the strongest solutions.[1] However, there has been a big problem: the storage of hydrogen.[2] Lightweight boron-containing compounds (sodium borohydride, ammonia borane, hydrazine borane, and so on) with high density of hydrogen have been extensively studied as promising solid chemical hydrogen storage materials over the last 15 years.[3] Among those, ammonia borane (H_3NBH_3, AB) and hydrazine borane ($N_2H_4BH_3$, HB) have 19.6 and 15.4 wt.% of hydrogen and surpass the US DOE 2015 targets.[4]

Both AB and HB can easily release their hydrogens at ambient temperature with appropriate catalyst systems by hydrolysis reactions as shown in Eq. (1) and Eq. (2):

$$H_3NBH_3(aq) + 2H_2(1) \xrightarrow{Catalyst} NH_4^+(aq)BO_2^-(aq) + 3H_2(g) \quad (1)$$

$$N_2H_4BH_3(aq)2H_2O(1) \xrightarrow{Catalyst} N_2H_5^+(aq)BO_2^-(aq) + 3H_2(g) \quad (2)$$

The first reports on the synthesis or hydrolysis of ammonia borane and hydrazine borane for hydrogen generation were published in 2006[5] and 2009[2], respectively. Since those years, a vast number of catalyst systems

*Correspondence: mrtrakap@gmail.com

have been employed for hydrogen release from hydrolysis of AB and HB. The lists of such types of pioneering catalyst systems recently used for the hydrolysis of AB and HB are shown in Tables 1 and 2, respectively. As

Table 1. Turnover frequency and activation energy values of various catalyst systems employed in hydrogen release from hydrolysis of AB.

Catalyst	TOF (mol H_2 mol catalyst^{-1} min^{-1})	Ea (kJ mol^{-1})	Reference
RuCuCo @ MIL-101	241.2	48	6
RuRh @ PVP NPs	386	47.4	7
Ni @ GO	2.1	-	8
Co @ GO	5.6	-	8
NiCo @ GO	6.8	-	8
AgCo @ PAMAM	15.8	35.7	9
RhNi @ ZIF-8	58.8	-	10
RuCuNi @ CNTs	311.2	36.7	11
Ru @ nanodiamond	229	50.7	12
AgPd @ UIO-66-NH_2	90	51.8	13
Ru @ MCM-41	288	41.6	14
AuCo @ CNT	36.1	38.8	15
Pd_xSn_{100-x}	13.6	27.2	16
$Cu_{75}Pd_{25}$	29.9	45	17
PdPt @ PVP NPs	125	51.7	18
PdRh @ PVP NPs	1333	46.1	19
Ru/g-C_3N_4	313	37.4	20
NiAgPd/C	93.8	38.4	21
NiPd @ rGO	28.7	45	22
Ru @ MIL-96	231	47.7	23
$Cu_{0.2}Ni_{0.8}$ @ MCM-41	10.7	38	24
AuCo @ CN	48.3	-	25
Co/?-Al_2O_3	-	62	26
CoPd/C	22.7	27.5	27
Ag @ Co/graphene	102.4	20.1	28
Co(0)/graphene	13.8	-	29
Co @ SiO_2	13.3	-	30
CoPd @ PVP NPs	30	48.6	This study

Table 2. Turnover frequency and activation energy values of various catalyst systems employed in hydrogen release from hydrolysis of HB.

Catalyst	TOF (mol H_2 mol catalyst^{-1} min^{-1})	Ea (kJ mol^{-1})	Reference
$Ni_{0.9}Pt_{0.1}$ @ graphene	4	-	31
Pd @ PVP NPs	42.9	54.5	32
NiPt @ CeO_2	3.9	-	33
PSSA-co-MA stabilized Co(0) NPs	6.2	60	34
PSSA-co-MA stabilized Ni(0) NPs	3.1	73	35
Rh @ HAP NPs	115	45	36
$RhCl_3$	100	44	37
CeO_x-RhNi @ rGO	11.1	-	38
Cu @ SiO_2	7.6	-	39
CoPd @ PVP NPs	45	50.6	This study

clearly seen from these tables, bimetallic/trimetallic catalysts containing noble metals (especially Ru, Rh, and Pt) have the highest catalytic activities in the hydrolysis reactions of AB and HB since the addition of a second element to monometallic catalysts will enhance the catalytic activities. However, catalyst systems with lower costs should be developed for the implementation of practical applications and therefore the hydrogen economy concept.

Here, we report for the first time the synthesis of poly(*N*-vinyl-2-pyrrolidone)-stabilized cobalt-palladium nanoparticles (CoPd @ PVP NPs) by an easy method, their characterization, and their use as active catalysts for hydrogen release from hydrolysis of AB and HB. Poly(*N*-vinyl-2-pyrrolidone), PVP, is one of the widely used stabilizers for the preparation of nanoparticles. Suitable cobalt and palladium salts have been coreduced by sodium borohydride ($NaBH_4$) in the presence of PVP as a stabilizer for the synthesis of CoPd @ PVP NPs. Very stable colloidal CoPd @ PVP nanoparticles have been characterized by UV-Vis spectroscopy, transmission electron microscopy-energy dispersive analysis (TEM-EDX), X-ray diffraction (XRD), and X-ray photoelectron spectroscopy (XPS). CoPd @ PVP nanoparticles, with the inclusion of cobalt in the structure, will be low-cost catalysts for hydrogen release from hydrolysis of AB and HB compared to the use of all-noble metal catalysts.

2. Results and discussion

2.1. Preparation and characterization of CoPd @ PVP nanoparticles

In order to prepare PVP-stabilized CoPd nanoparticles, suitable palladium and cobalt salts were simultaneously reduced in aqueous solution by $NaBH_4$ in the presence of PVP as a stabilizer. With a fast reduction of corresponding metal salts the solution turned black, indicating that Co^{2+} and Pd^{2+} ions were converted to Co^0 and Pd^0. This conversion can be best followed by UV-Vis spectroscopy. Spectral changes during CoPd @ PVP nanoparticle formation from simultaneous reduction of cobalt and palladium salts by $NaBH_4$ are shown in Figure 1. One can easily see the disappearance of d-d transition peaks of Co^{2+} and Pd^{2+} ions by complete reduction of these ions to form CoPd @ PVP nanoparticles.

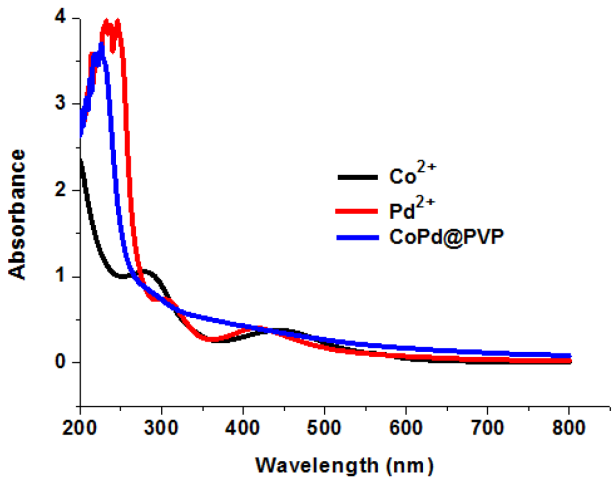

Figure 1. UV-Vis spectra of cobalt(II) chloride hexahydrate ($CoCl_2 \bullet 6H_2O$), potassium tetrachloropalladate(II) (K_2PdCl_4), and CoPd @ PVP nanoparticles.

The particle size and the crystallinity of the CoPd @ PVP nanoparticles was determined by TEM and XRD analysis. The TEM image taken at 50 nm magnification is shown in Figure 2a. From this image, 125

particles were counted and the mean particle size was found to be 4.4 ± 1.1 nm. Figure 2b shows the XRD pattern of CoPd @ PVP nanoparticles. The peak observed at $2\theta = 40.2^\circ$ belongs to the (111) plane of face-centered cubic CoPd. The slight shift to the higher 2θ value from the (111) plane of fcc - Pd ($2\theta = 39.7^\circ$) confirms the alloy structure formation in CoPd @ PVP nanoparticles.[40]

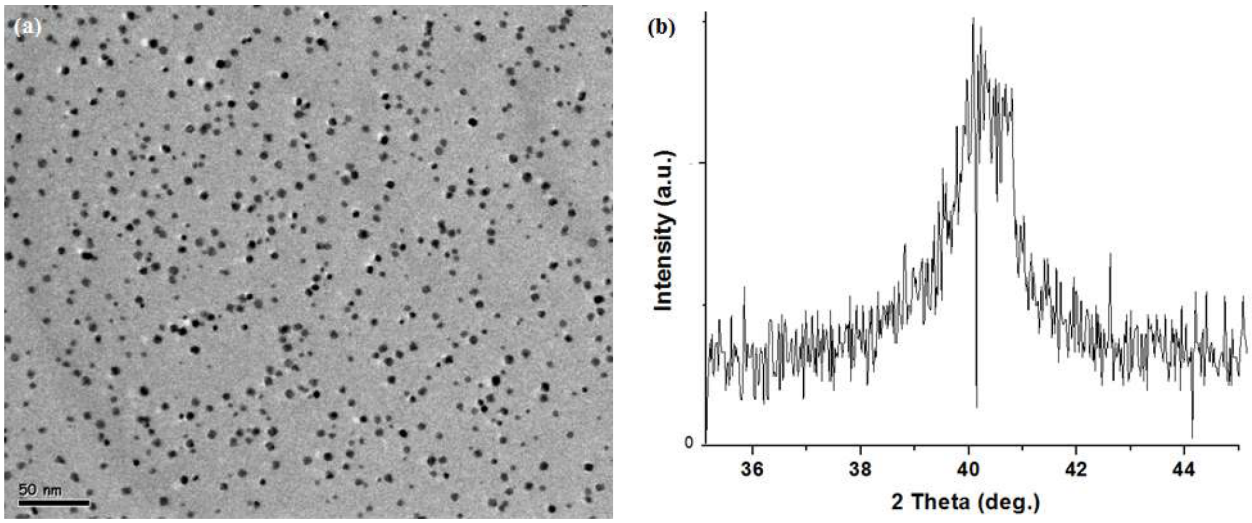

Figure 2. a) TEM picture of CoPd @ PVP nanoparticles taken at 50 nm magnification. b) XRD pattern of CoPd @ PVP nanoparticles, showing the pattern of the (111) plane.

High-resolution XPS spectra for Co 2p and Pd 3d regions for CoPd @ PVP nanoparticles are shown in Figure 3. In Figure 3a, absorption bands located at 795.1 and 779.1 eV are assigned to Co(0) $2p_{1/2}$ and Co(0) $2p_{3/2}$, respectively.[41] There are also CoO (785.5 eV) and CoO_x (801.5 eV) species in the catalyst. In Figure 3b, two bands located at 338.6 eV and 333.3 eV are assigned to Pd(0) $3d_{3/2}$ and Pd(0) $3d_{5/2}$, respectively.[42] There is also a small amount of PdO (335.1 eV) species in the catalyst. The slight binding energy shifts to lower values also confirm the alloy formation in the CoPd @ PVP nanoparticles.

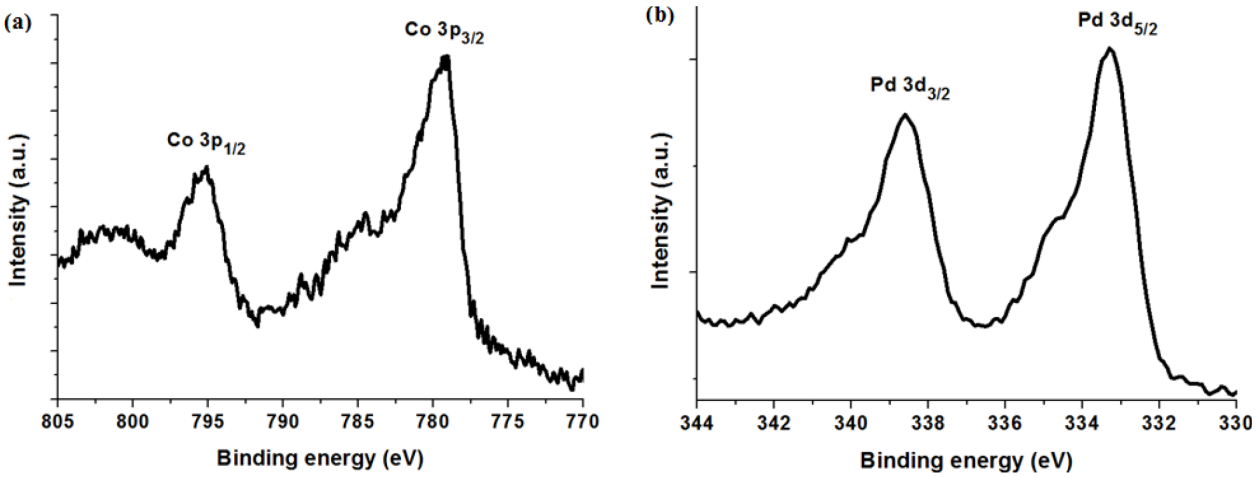

Figure 3. High-resolution X-ray photoelectron spectrum of CoPd @ PVP nanoparticles, showing a) Co 2p and b) Pd 3d regions.

2.2. Kinetics of CoPd @ PVP nanoparticle-catalyzed hydrolysis of AB and HB

CoPd @ PVP nanoparticles are effective catalysts for the hydrolysis of AB and HB. The plots of mol H_2/mol H_3NBH_3 (n H_2/n AB) against time for the hydrolysis of 100 mM H_3NBH_3 solutions by CoPd @ PVP nanoparticles at catalyst concentrations of 1.0 mM to 5.0 mM (1.0, 2.0, 3.0, 4.0, 5.0) at 25.0 ± 0.1 °C are shown in Figure 4a. The immediate hydrogen release starts quickly and goes on to the complete hydrolysis of AB. The rates of hydrogen release obtained from the linear parts of the plots in Figure 4a were plotted against catalyst concentration and a straight line that has a slope of 1.123 was acquired for the hydrolysis of AB as shown in Figure 4b. These results indicate that the hydrolysis reaction of AB has first-order dependency on catalyst concentration.

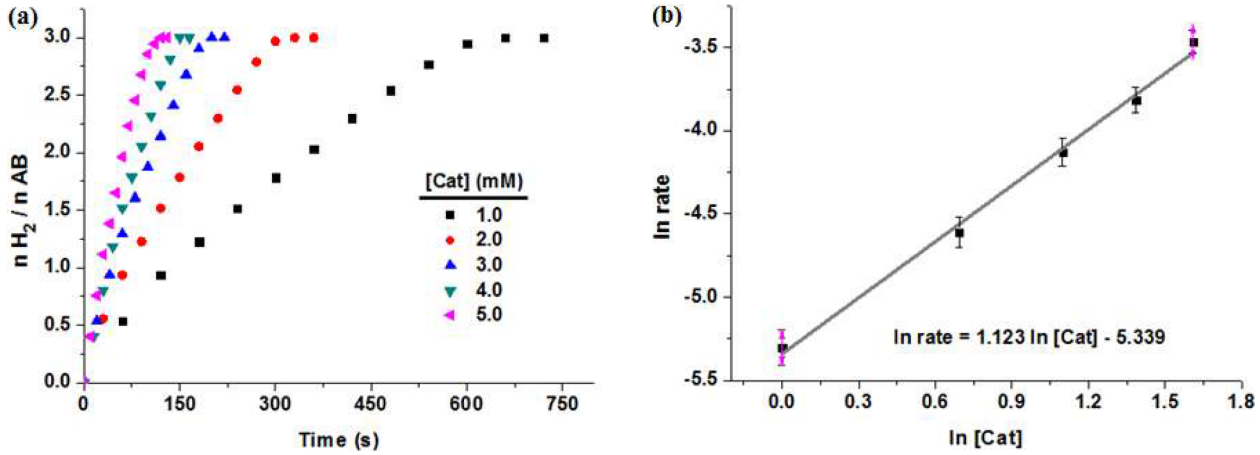

Figure 4. a) Plots of mol H_2/mol H_3NBH_3 versus time for the hydrolysis of 100 mM H_3NBH_3 catalyzed by CoPd @ PVP nanoparticles at different catalyst concentrations (1.0, 2.0, 3.0, 4.0, and 5.0 mM) at 25.0 ± 0.1 °C. b) Plots of the hydrogen release rate versus the catalyst concentration in the hydrolysis of H_3NBH_3 catalyzed by CoPd @ PVP nanoparticles at different catalyst concentrations.

Similarly, the plots mol H_2/mol $N_2H_4BH_3$ (n H_2/n HB) against time for the hydrolysis of 100 mM $N_2H_4BH_3$ solutions by CoPd @ PVP nanoparticles at catalyst concentrations of 1.5 mM to 3.5 mM (1.5, 2.0, 2.5, 3.0, 3.5) at 25.0 ± 0.1 °C are shown in Figure 5a. Again, there is quick hydrogen release and it goes on to complete hydrolysis of HB. It is noteworthy that two types of hydrolysis/decomposition reactions for HB can be found in the literature: in the first and most common one, HB gives up to 3 mol of hydrogen gas by hydrolysis of the BH_3 group, and in the second type, HB yields up to 6 mol of gas (5 mol of hydrogen and 1 mol of nitrogen gases) upon decomposition of the N_2H_4 group in addition to the hydrolysis of the BH_3 group. Our study falls into the first category since the second type of reactions can only be found in the presence of nickel-based bimetallic catalysts.[43–46]

The rates of hydrogen release obtained from the linear parts of the plots in Figure 5a were plotted against catalyst concentration and a straight line that has a slope of 1.174 was acquired for the hydrolysis of HB, as shown in Figure 5b. These results indicate that the hydrolysis reaction of HB also has first-order dependency on catalyst concentration. The hydrolysis reactions of AB and HB were found to have no dependency on H_3NBH_3 and $N_2H_4BH_3$ substrate concentrations. Therefore, they proceed via zeroth order with respect to substrate concentration. In light of these combined kinetic results, rate laws for the hydrolysis of H_3NBH_3 and $N_2H_4BH_3$ are given in Eq. (3) and Eq. (4):

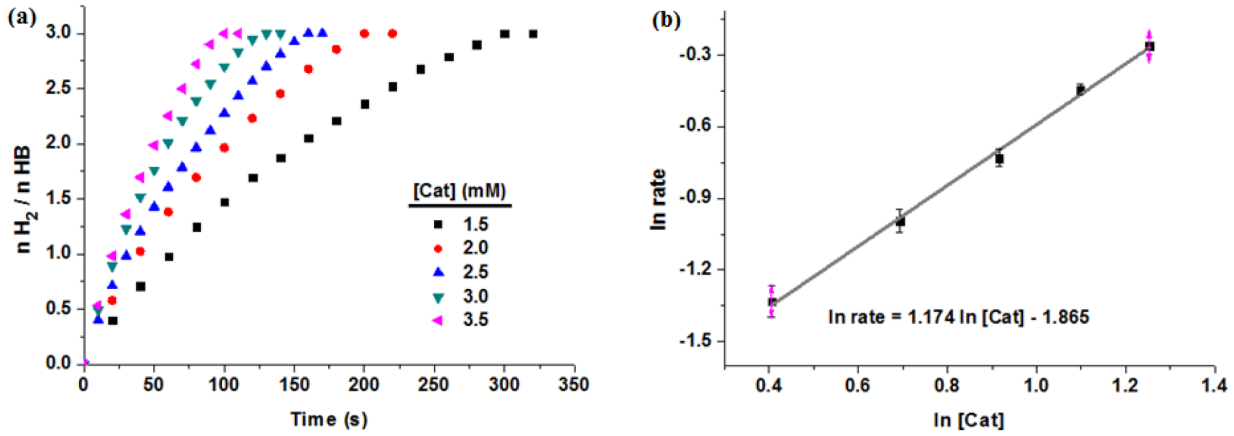

Figure 5. a) Plots of mol H_2/mol $N_2H_4BH_3$ versus time for the hydrolysis of 100 mM $N_2H_4BH_3$ catalyzed by CoPd @ PVP nanoparticles at different catalyst concentrations (1.5, 2.0, 2.5, 3.0, and 3.5 mM) at 25.0 ± 0.1 °C. b) Plots of the hydrogen release rate versus the catalyst concentration in the hydrolysis of $N_2H_4BH_3$ catalyzed by CoPd @ PVP nanoparticles at different catalyst concentrations.

$$\frac{-3d[NH_3BH_3]}{dt} = \frac{d[H_2]}{dt} = k[Catalyst] \tag{3}$$

$$\frac{-3d[N_2H_4BH_3}{dt} = \frac{d[H_2]}{dt} = k[Catalyst] \tag{4}$$

2.3. Determination of energies of activation for AB and HB hydrolysis reactions catalyzed by CoPd @ PVP nanoparticles

In order to obtain the activation energies, CoPd @ PVP nanoparticle-catalyzed hydrolysis reactions of AB and HB were performed at different temperature values. The plots of mol H_2/mol H_3NBH_3 (n H_2/n AB) and mol H_2/mol $N_2H_4BH_3$ (n H_2/n HB) against time for the hydrolysis of 100 mM H_3NBH_3 and 100 mM $N_2H_4BH_3$ catalyzed by CoPd @ PVP nanoparticles (3.0 mM for hydrolysis of AB and 2.5 mM for hydrolysis of HB) at various temperatures from 5 °C to 30 °C (10, 15, 20, 25, 30 °C for hydrolysis of AB and 5, 10,15, 20, 25 °C for hydrolysis of HB) are shown in Figures 6a and 6b, respectively. Complete hydrogen release (3.0 mol H_2/mol H_3NBH_3 and 3.0 mol H_2/mol $N_2H_4BH_3$) for the hydrolysis reactions of AB and HB are obtained by CoPd @ PVP nanoparticles (3.0 mM for hydrolysis of AB and 2.5 mM for hydrolysis of HB) within 200 s and 160 s, respectively, at 25.0 ± 0.1 °C. They correspond to average TOF values of 30 min^{-1} and 45 min^{-1}. The average TOF value of CoPd @ PVP nanoparticles in the hydrolysis of AB is lower than that of noble metals like Ru, Rh, or Pt but still much higher than that of NiCo @ GO (6.8 min^{-1}),[8] AgCo @ PAMAM (15.8 min^{-1}),[9] Pd_xSn_{100-x} (13.6 min^{-1}),[16] $Cu_{75}Pd_{25}$ (29.9 min^{-1}),[17] NiPd @ rGO (28.7 min^{-1}),[22] and $Cu_{0.2}Ni_{0.8}$ @ MCM-41 (10.7 min^{-1}),[24] as seen from Table 1. Similarly, the average TOF value of CoPd @ PVP nanoparticles in the hydrolysis of HB is lower than that of Rh @ HAP NPs (115 min^{-1})[36] and $RhCl_3$ (100 min^{-1})[37] but higher than that of $Ni_{0.9}Pt_{0.1}$ @ graphene (4 min^{-1}),[31] Pd @ PVP NPs (42.9 min^{-1}),[32] NiPt @ CeO_2 (3.9 min^{-1}),[33] PSSA-co-MA stabilized Co(0) NPs (6.2 min^{-1}),[34] PSSA-co-MA stabilized Ni(0) NPs (3.1 min^{-1}),[35] CeO_x-RhNi @ rGO (11.1 min^{-1}),[38] and Cu @ SiO_2 (7.6 min^{-1}),[39] as seen from Table 2.

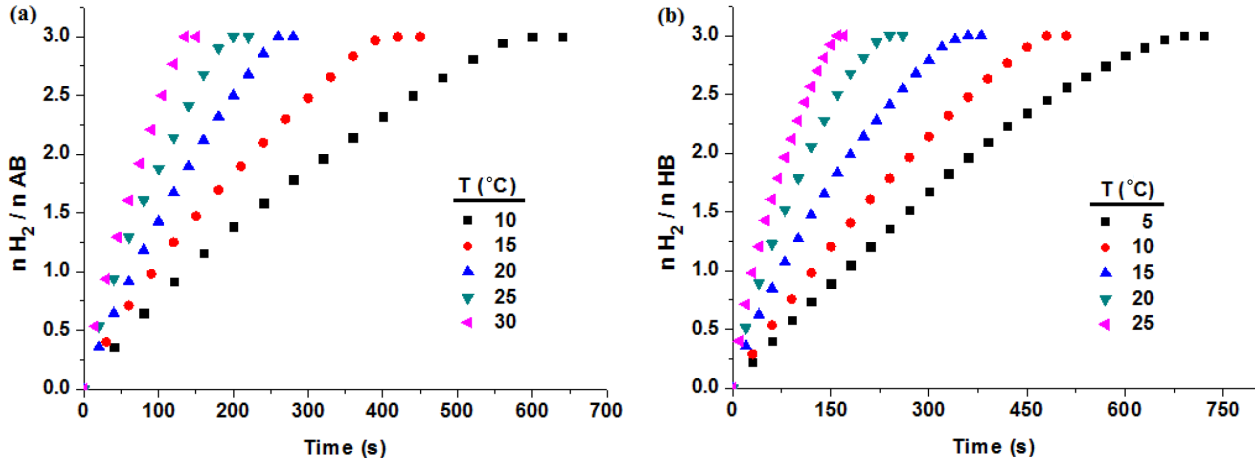

Figure 6. Plots of a) mol H_2/mol H_3NBH_3 versus time in the hydrolysis of 100 mM of H_3NBH_3 catalyzed by CoPd @ PVP (3.0 mM) at various temperatures (10, 15, 20, 25, and 30 °C) and b) mol H_2/mol $N_2H_4BH_3$ versus time in the hydrolysis of 100 mM $N_2H_4BH_3$ catalyzed by CoPd @ PVP (2.5 mM) at various temperatures (5, 10, 15, 20, and 25 °C).

The observed rate constants (k_{obs}) for hydrogen release from hydrolysis reactions of AB and HB were calculated from the linear parts of the plots given in Figure 6 and are shown in Tables 3 and 4, respectively. They were used to calculate the activation energies (E_a = 48.6 ± 2 and 50.6 ± 2 kJ mol^{-1} for H_3NBH_3 and $N_2H_4BH_3$) from Arrhenius plots shown in Figures 7a and 7b for the hydrolysis reactions of H_3NBH_3 and $N_2H_4BH_3$, respectively.

Table 3. The observed rate constant values, k_{obs}, for the hydrolysis of AB starting with a solution of 100 mM of NH_3BH_3 and 3.0 mM of CoPd @ PVP nanoparticles catalyst at different temperatures.

T (K)	k_{obs} (mmol H_2 (mmol catalyst)$^{-1}$ s^{-1})
283	0.19133
288	0.26933
293	0.42000
298	0.53567
303	0.74400

Table 4. The observed rate constant values, k_{obs}, for the hydrolysis of HB starting with a solution of 100 mM of $N_2H_4BH_3$ and 2.5 mM of CoPd @ PVP nanoparticles catalyst at different temperatures.

T (K)	k_{obs} (mmol H_2 (mmol catalyst)$^{-1}$ s^{-1})
278	0.21104
283	0.27900
288	0.40736
293	0.61608
298	0.89284

The energy of activation value of CoPd @ PVP nanoparticles in the hydrolysis of AB is higher than that of RuCuCo @ MIL-101 (48 kJ mol^{-1}),[6] RuCuNi @ CNTs (36.7 kJ mol^{-1}),[11] AuCo @ CNT (38.8 kJ mol^{-1}),[15] and NiAgPd/C (38.4 kJ mol^{-1}),[21] but lower than that of Ru @ nanodiamond (50.7 kJ mol^{-1}),[12]

AgPd @ UIO-66-NH_2 (51.8 kJ mol^{-1}),[13] and PdPt @ PVP NPs (51.7 kJ mol^{-1}),[18] as seen from Table 1. Similarly, the energy of activation value of CoPd @ PVP nanoparticles in the hydrolysis of HB is higher than that of Rh @ HAP NPs (45 kJ mol^{-1})[36] and $RhCl_3$ (44 kJ mol^{-1})[37] but lower than that of Pd @ PVP NPs (54.5 kJ mol^{-1}),[32] PSSA-co-MA stabilized Co(0) NPs (60 kJ mol^{-1}),[34] and PSSA-co-MA stabilized Ni(0) NPs (73 kJ mol^{-1}),[35] as clearly seen from Table 2.

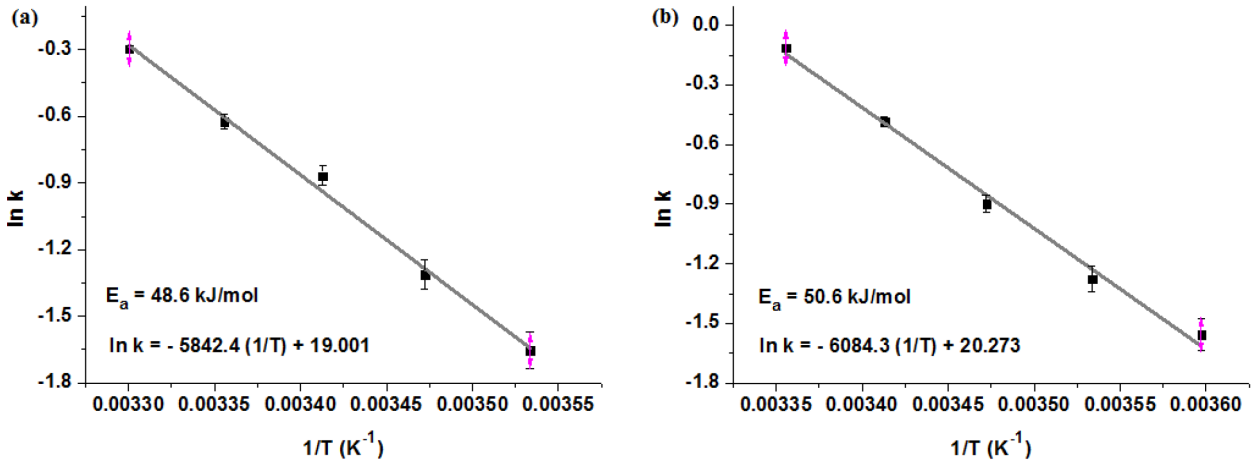

Figure 7. Arrhenius plots for the hydrolysis of a) H_3NBH_3 (100 mM) catalyzed by CoPd @ PVP nanoparticles (3.0 mM) and b) $N_2H_4BH_3$ (100 mM) catalyzed CoPd @ PVP nanoparticles (2.5 mM).

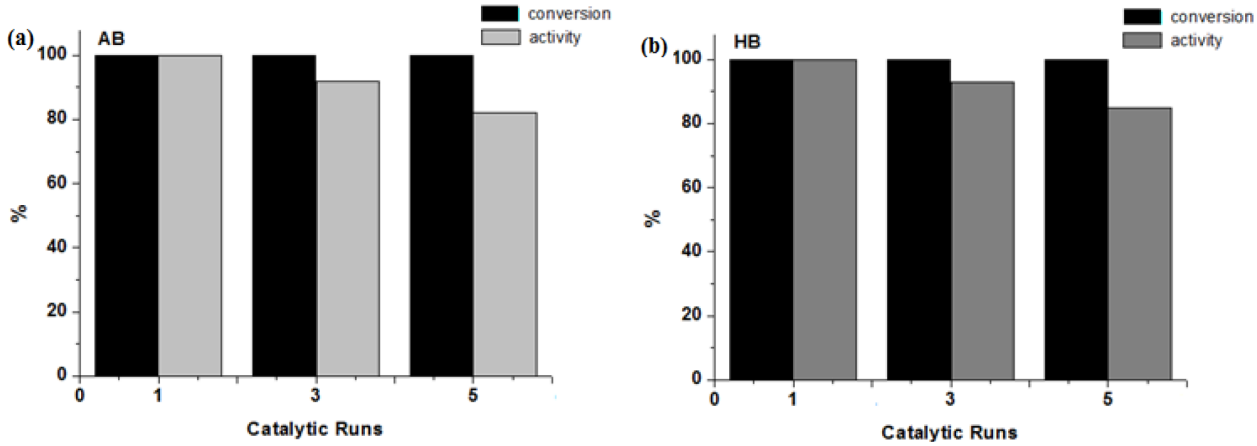

Figure 8. Durabilities of CoPd @ PVP nanoparticles in the hydrolysis of a) H_3NBH_3 (100 mM) and b) $N_2H_4BH_3$ (100 mM) at 25.0 ± 0.1 °C, in terms of % conversion of AB and HB and retained % catalytic activity of CoPd @ PVP nanoparticles.

2.4. The durabilities of CoPd @ PVP nanoparticles in the hydrolysis of AB and HB

The CoPd @ PVP nanoparticles were found to be durable catalysts in the hydrolysis of AB and HB by carrying out a series of experiments that included consecutive additions of H_3NBH_3 and $N_2H_4BH_3$ after the first runs of hydrolysis reactions. CoPd @ PVP nanoparticles keep 82% and 85% of their initial activity in the hydrolysis of H_3NBH_3 and $N_2H_4BH_3$ after the fifth run as shown in Figures 8a and 8b, respectively. The

small decreases in the catalytic performance of CoPd @ PVP nanoparticles in both hydrolysis reactions are due to the nanoparticles' surface passivation by rising concentration of metaborate, which blocks the accessibility of active sites,[47] since there is no change in the structure of the catalyst proved by TEM analysis after durability tests.

3. Experimental

3.1. Chemicals

Potassium tetrachloropalladate(II) (K_2PdCl_4), cobalt(II) chloride hexahydrate ($CoCl_2 \bullet 6H_2O$), hydrazine hemisulfate ($N_2H_4 0.5H_2SO_4$), ammonia borane, poly(*N*-vinyl-2-pyrrolidone), sodium borohydride, and 1,4-dioxane were all purchased from Sigma-Aldrich. Deionized water was distilled by the Milli-Q pure WS water purification system. All glassware and Teflon-coated magnetic stirring bars were washed with acetone and distilled water and dried in the oven at 120 °C.

3.2. Synthesis and characterization of HB

HB ($N_2H_4BH_3$) has been synthesized from the reaction between hydrazine hemisulfate and sodium borohydride in dioxane employing the literature procedures.[48,49] The melting point of HB is about 60 °C. All spectral data for HB are in good agreement with the values reported in the literature.[49]

3.3. Synthesis of CoPd @ PVP nanoparticles

CoPd @ PVP nanoparticles were synthesized from the simultaneous reduction of suitable cobalt and palladium salts in aqueous solution by $NaBH_4$ in the presence of poly(*N*-vinyl-2-pyrrolidone) as a stabilizer. To an aqueous solution of cobalt(II), chloride hexahydrate (0.10 mmol), potassium tetrachloropalladate(II) (0.10 mmol), and PVP (55 mg) in 15 mL of deionized H_2O, an aqueous solution of $NaBH_4$ (25 mg) in 5 mL of deionized H_2O was added. Both metals were easily reduced to form PVP-stabilized CoPd nanoparticles as a stable black colloidal solution.

3.4. Characterization of CoPd @ PVP nanoparticles

UV-Vis spectra of the CoPd @ PVP nanoparticles were recorded on a Cary 5000 (Varian) UV-Vis spectrophotometer. TEM analysis of CoPd @ PVP nanoparticles was performed with a JEOL-2010 microscope operating at 200 kV, fitted with a LaB_6 filament and with lattice and theoretical point resolutions of 0.14 nm and 0.23 nm. The sizes of the particles were calculated from enlarged photographs. XRD analysis was carried out on a Rigaku Ultima IV X-Ray Diffractometer. The XPS spectrum of the CoPd @ PVP nanoparticles was obtained by SPECS spectrometer equipped with a hemispherical analyzer and using monochromatic Mg-Kα radiation (1250 eV, the X-ray tube working at 15 kV and 350 W). ^{11}B NMR spectra were recorded on a Bruker Avance DPX 400 MHz spectrometer.

3.5. Catalytic evaluation of CoPd @ PVP nanoparticles in the hydrolysis of AB and HB

The catalytic performances of CoPd @ PVP nanoparticles in the hydrolysis reactions of AB and HB were defined by determining the hydrogen generation rates. In all experimental studies, a jacketed reaction flask containing a Teflon-coated stirring bar was put on a magnetic stirrer and thermostated to 25.0 ± 0.1 °C by circulating water through its jacket. Afterwards, a graduated glass tube filled with water was connected to the reaction flask to measure the volume of the evolved hydrogen gas from the hydrolysis reaction. In an ordinary experiment,

31.8 mg (1.0 mol) of H_3NBH_3 or 46.0 mg (1.0 mmol) of $N_2H_4BH_3$ was dissolved in x mL of deionized water. This solution was transferred with a glass pipette into the reaction flask. Known amounts of CoPd @ PVP nanoparticles (10.0 – x mL) were then added to the reaction mixture. The experiment was started by closing the flask and the volume of evolved hydrogen gas was determined by recording the displacement of the water level. Additionally, the conversions of ammonia borane (δ= –23.9 ppm) to metaborate (δ= 9 ppm) and of hydrazine borane (δ= –20 ppm) to hydrazinium metaborate (δ= 12.5 ppm) were also controlled by ^{11}B NMR spectroscopy.

3.6. Kinetic study of the CoPd @ PVP nanoparticle-catalyzed hydrolysis of AB and HB

The rate laws for the CoPd @ PVP nanoparticle-catalyzed hydrolysis reactions of AB and HB were established by performing two different experimental sets by following the same procedure described in the previous section. In the first set, substrate concentration was constant at 100 mM for AB and HB while CoPd @ PVP nanoparticle catalyst concentrations were changed from 1.0 mM to 5.0 mM (1.0, 2.0, 3.0, 4.0, 5.0 mM for hydrolysis of AB and 1.5, 2.0, 2.5, 3.0, 3.5 mM for hydrolysis of HB). In the second set, CoPd @ PVP nanoparticle catalyst concentration was constant (3.0 mM for hydrolysis of AB and 2.5 mM for hydrolysis of HB) and substrate concentrations were changed from 40 mM to 120 mM (40, 60, 80, 100, 120).

3.7. Activation energies for the CoPd @ PVP nanoparticle-catalyzed hydrolysis of AB and HB

To determine the activation energies for the CoPd @ PVP nanoparticle-catalyzed hydrolysis reactions of AB and HB, hydrolysis reactions were carried out using known amounts of substrate (100 mM) and CoPd @ PVP nanoparticles (3.0 mM for hydrolysis of AB and 2.5 mM for hydrolysis of HB) following the same procedure described in Section 3.5 at different temperatures from 5 °C to 30 °C (10, 15, 20, 25, 30 °C for hydrolysis of AB and 5, 10,15, 20, 25 °C for hydrolysis of HB). The observed rate constant (k_{obs}) values for catalytic hydrolysis reactions of AB and HB were used to calculate the activation energies (E_a) of CoPd @ PVP nanoparticles for the hydrolysis of both substrates.

3.8. Durability tests for the CoPd @ PVP nanoparticles in the hydrolysis of AB and HB

The durabilities of CoPd @ PVP nanoparticles in the hydrolysis of AB and HB were determined by a series of experimental procedures starting with 10.0 mL of solution containing CoPd @ PVP nanoparticles (3.0 mM for hydrolysis of AB and 2.5 mM for hydrolysis of HB) and 100 mM H_3NBH_3 (or $N_2H_4BH_3$) at 25.0 ± 0.1 °C. After the complete hydrolysis reactions, new equivalents of H_3NBH_3 (or $N_2H_4BH_3$) substrate were added to the mixture quickly. The results of the durability tests were given as % initial CoPd @ PVP nanoparticle catalytic activity and % conversions of AB and HB against the number of catalytic cycles in the hydrolysis of H_3NBH_3 and $N_2H_4BH_3$.

4. Conclusions

In this study, we synthesize, characterize, and employ CoPd @ PVP nanoparticles as active catalysts in hydrolysis reactions of AB and HB. The following conclusions are obtained from this research:

- CoPd @ PVP nanoparticles are synthesized from simultaneous reduction of suitable cobalt and palladium salts by $NaBH_4$ in the presence of PVP as a stabilizer.

- CoPd @ PVP nanoparticles are active catalysts for hydrogen release from the hydrolysis of AB and HB.
- Average TOF values of 30 min^{-1} and 45 min^{-1} are provided by CoPd @ PVP nanoparticles in the hydrolysis of AB and HB, respectively.
- Activation energies for CoPd @ PVP nanoparticle-catalyzed hydrolysis of AB and HB are 48.6 $\pm$ 2 and 50.6 $\pm$ 2 kJ mol^{-1}, respectively.

Acknowledgments

This work was supported by the Research Fund of Yüzüncü Yıl University (Project Number: 2014-DNZ-B202). The TEM, XRD, and XPS analyses were performed at the Central Laboratory of METU.

References

1. Rand, D. A. J.; Dell, R. M. *J. Power Sources* **2005**, *144*, 568-578.
2. Hügle, T.; Kühnel, M. F.; Lentz, D. *J. Am. Chem. Soc.* **2009**, *131*, 7444-7446.
3. Lu, Z. H.; Yao, Q.; Zhang, Z.; Yang, Y.; Chen, X. *J. Nanomater.* **2014**, *2014*, 729029.
4. US Energy Information Administration. *Annual Energy Outlook 2005 with Projections to 2025*; EIA: Washington, DC, USA, 2005.
5. Chandra, M.; Xu, Q. *J. Power Sources* **2006**, *156*, 190-194.
6. Yang, K.; Zhou, L.; Xiong, X.; Ye, M.; Li, L.; Xia, Q. *Microporous Mesoporous Mater.* **2016**, *225*, 1-8.
7. Rakap, M. *J. Alloys Compd.* **2015**, *649*, 1025-1030.
8. Zhao, B.; Liu, J.; Zhou, L.; Long, D.; Feng, K.; Sun, X.; Zhong, J. *Appl. Surf. Sci.* **2016**, *362*, 79-85.
9. Ke, D.; Li, Y.; Wang, J.; Zhang, L.; Wang, J.; Zhao, X.; Yang, S.; Han, S. *Int. J. Hydrogen Energy* **2016**, *41*, 2564-2574.
10. Xia, B.; Liu, C.; Wu, H.; Luo, W.; Cheng, G. *Int. J. Hydrogen Energy* **2015**, *40*, 16391-16397.
11. Xiong, X.; Zhou, L.; Yu, G.; Yang, K.; Ye, M.; Xia, Q. *Int. J. Hydrogen Energy* **2015**, *40*, 15521-15528.
12. Fan, G.; Liu, Q.; Tang, D.; Li, X.; Bi, J.; Gao, D. *Int. J. Hydrogen Energy* **2016**, *41*, 1542-1549.
13. Shang, N. Z.; Feng, C.; Gao, S. T.; Wang, C. *Int. J. Hydrogen Energy* **2016**, *41*, 944-950.
14. Luo, W.; Cai, P.; Cheng, G. Z. *Chin. Chem. Lett.* **2015**, *26*, 1345-1350.
15. Kang, K.; Gu, X.; Guo, L.; Liu, P.; Sheng, X; Wu, Y.; Cheng, J.; Su, H. *Int. J. Hydrogen Energy* **2015**, *40*, 12315-12324.
16. Li, Y.; Dai, Y.; Tian, X. *Int. J. Hydrogen Energy* **2015**, *40*, 9235-9243.
17. Güngörmez, K.; Metin, Ö. *Appl. Catal. A-Gen.* **2015**, *494*, 22-28.
18. Rakap, M. *J. Power Sources* **2015**, *276*, 320-327.
19. Rakap, M. *Appl. Catal. B-Environ.* **2015**, *163*, 129-134.
20. Fan, Y.; Li, X.; He, X.; Zeng, C.; Fan, G.; Liu, Q.; Tang, D. *Int. J. Hydrogen Energy* **2014**, *39*, 19982-19989.
21. Hu, L.; Zheng, B.; Lai, Z.; Huang, K. W. *Int. J. Hydrogen Energy* **2014**, *39*, 20031-20037.
22. Çiftçi, N. S.; Metin, Ö. *Int. J. Hydrogen Energy* **2014**, *39*, 18863-18870.
23. Wen, L.; Su, J.; Wu, X.; Cai, P.; Luo, W.; Cheng, G. *Int. J. Hydrogen Energy* **2014**, *39*, 17129-17135.
24. Lu, Z. H.; Li, J.; Feng, G.; Yao, Q.; Zhang, F.; Zhou, R.; Tao, D.; Chen, X.; Yu, Z. *Int. J. Hydrogen Energy* **2014**, *39*, 13389-13395.

25. Guo, L. T.; Cai, Y. Y.; Ge, J. M.; Zhang, Y. N.; Gong, L. H.; Li, X. H.; Wang, K. X.; Ren, Q. Z.; Su, J.; Chen, J. S. *ACS Catal.* **2015**, *5*, 388-392.
26. Xu, Q.; Chandra, M. *J. Power Sources* **2006**, *163*, 364-370.
27. Sun, D.; Mazumder, V.; Metin, Ö.; Sun, S. *ACS Nano* **2011**, *5*, 6458-6464.
28. Yang, L.; Luo, W.; Cheng, G. *ACS Appl. Mater. Interfaces* **2013**, *5*, 8231-8240.
29. Yang, L.; Cao, N.; Du, C.; Dai, H.; Hu, K.; Luo, W.; Cheng, G. *Mater. Lett.* **2014**, *115*, 113-116.
30. Metin, Ö.; Dinç, M.; Eren, Z. S.; Özkar, S. *Int. J. Hydrogen Energy* **2011**, *36*, 11528-11535.
31. Zhang, Z.; Lu, Z. H.; Chen, X. *ACS Sustainable Chem. Eng.* **2015**, *3*, 1255-1261.
32. Tunç, N.; Abay, B.; Rakap, M. *J. Power Sources* **2015**, *299*, 403-407.
33. Zhang, Z.; Wang, Y.; Chen, X.; Lu, Z. H. *J. Power Sources* **2015**, *291*, 14-19.
34. Karahan, S.; Özkar, S. *Int. J. Hydrogen Energy* **2015**, *40*, 2255-2265.
35. Şencanlı, S.; Karahan, S.; Özkar, S. *Int. J. Hydrogen Energy* **2013**, *38*, 14693-14703.
36. Çelik, D.; Karahan, S.; Zahmakıran, M.; Özkar, S. *Int. J. Hydrogen Energy* **2012**, *37*, 5143-5151.
37. Karahan, S.; Zahmakıran, M.; Özkar, S. *Int. J. Hydrogen Energy* **2011**, *36*, 4958-4966.
38. Zhang, Z.; Lu, Z. H.; Tan, H.; Chen, X.; Yao, Q. J. *Mater. Chem. A* **2015**, *3*, 23520-23529.
39. Yao, Q.; Lu, Z. H.; Zhang, Z.; Chen, X.; Lan, Y. *Sci. Rep.* **2014**, *4*, 7597.
40. Göksu, H.; Can, H.; Şendil, K.; Gültekin, M. S.; Metin, Ö. *Appl. Catal. A-Gen.* **2014**, *488*, 176-182.
41. Mandale, A. B.; Badrinarayanan, S.; Date, S. K.; Sinha, A. P. B. *J. Electron Spectrosc. Relat. Phenom.* **1984**, *33*, 61-72.
42. Rakap, M.; Özkar, S. *Int. J. Hydrogen Energy* **2010**, *35*, 1305-1312.
43. Çakanyıldırım, Ç.; Demirci, U. B.; Şener, T.; Xu, Q.; Miele, P. *Int. J. Hydrogen Energy* **2012**, *37*, 9722-9729.
44. Hannauer, J.; Demirci, U. B.; Geantet, C.; Herrmann, J. M.; Miele, P. *Int. J. Hydrogen Energy* **2012**, *37*, 10758-10767.
45. Zhu, Q. L.; Zhong, D. C.; Demirci, U. B.; Xu, Q. *ACS Catal.* **2014**, *4*, 4261-4268.
46. Zhang, Z.; Lu, Z. H.; Chen, X. *ACS Sustainable Chem. Eng.* **2015**, *3*, 1255-1261.
47. Clark, T. J.; Whittell, G. R.; Manners, I. *Inorg. Chem.* **2007**, *46*, 7522-7527.
48. Moury, R.; Moussa, G.; Demirci, U. B.; Hannauer, J.; Bernard, S.; Petit, E.; van der Lee, A.; Miele, P. *Phys. Chem. Chem. Phys.* **2012**, *14*, 1768-1777.
49. Gunderloy, F. C. *Inorg. Synth.* **1967**, *9*, 13-16.